Interaction between Dust and Fission Products in Primary Circuit of HTGR

Sung Deok Hong[*], Nam-il Tak, Eung Seon Kim, Min Hwan Kim
Korea Atomic Energy Research Institute, Yuseong-Gu, Daejeon, Korea, 305-600
[*]*Corresponding author: sdhong1@kaeri.re.kr*

1. Introduction

The knowledge of the behaviour of fission products (FPs) in the primary circuits of high temperature reactors is very important for the prediction of the potential hazard for operators during maintenance and for the environment at a reactor accident. In case of pressure loss accidents, a considerable amount of fission products could be transported from the pressure vessel into the containment by dusts which might be blown out during depressurization. In this paper the behaviour of the dust and the interaction between fission products and dust particles is discussed in details.

The suspended dust, previously formed in the reactor coolant system (RCS) by various reactions, is the carrier that moves the FP out of the core. In general, the dust is much larger than the FP and will be distributed at various sizes (i.e., a polydispersed distribution). The fission products generated from fission are of nano-sized diameters while the dusts are of micro-sized diameters. Their interactions are illustrated schematically in Fig. 1. As shown in Fig. 1, small FPs will be captured by dust with both adsorption and diffusion processes and will be departed from the dust with both desorption and evaporation processes. Collisions of dust particles with fission products can be also occur. There are two factors that make the interaction complicated. One is diverse forms of both FP and dust. The diversity of the FP, is determined by its unique physico-chemical properties while diversity of dust is due to its various sizes as well as the substances it contains. The other factor, which is the concentration of the dust, depends on the part of the primary system of the reactor in which the dust is located. In addition, this factor is affected if the design of the reactor core and the RCS system differ.

2. Fission Products

The radionuclide containment system for an HTGR consists of multiple barriers to limit the release of radionuclides from the core into the environment to insignificant levels during normal operation and a spectrum of postulated accidents. The three release barriers considered within the scope of safety analyses are: (1) the particle coatings, particularly the SiC coating (2) the primary coolant pressure boundary; and (3) the reactor building/containment. The transport behaviour of radionuclides during core heats up accidents in HTGRs is much simpler than that in LWRs [2]. Relatively few radionuclides (primarily, radioisotopes of Kr, Xe, I, Te, Ag, Cs and Sr) are released from the core. No heavy metals or core structural materials are released, and the radionuclide mass concentrations are so low that aerosols are not expected to form. Table I summarizes the anticipated forms of the FPs and their potential release behaviour [2, 3, 4].

3. Dust

3.1 Generation

The radionuclide containment system for an HTGR consists of multiple. Dust can be generated by abrasion, gas-to-particle conversion, degradation of the insulation, and radiation damage, among other pathways. Recent experiments have indicated that the carbonaceous dust particles produced by graphite abrasion can be highly irregular, and this may be true of particles generated by other mechanisms as well [5, 6]. It has also been found that graphite particles can be highly porous with very large surface areas, making dust-facilitated FP transport a major factor. Dust samples collected in the VAMPYR-II in fine dust filters preceding the fission product filters, contain a significant amount of metallic particles as shown in Table II [3].
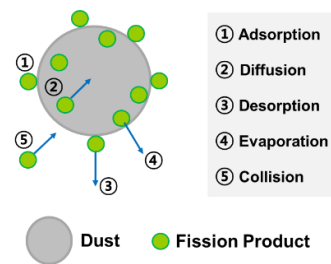
Fig. 1. Schematic illustration of FP-dust interaction [1].

Table I: Interaction of FPs in both Core and Primary loop.

Key FP	Interaction in core	Interaction in primary
I-131	Retained by PyC/SiC	Deposits on metals
Cs-137	Retained by SiC Matrix/graphite retention	Deposits on metals/dust
Sr-90	Matrix/graphite retention	Deposits on metals/dust
Ag-110m	Permeates intact SiC	Deposits on metals
Te-132	Retained by PyC/SiC	Deposits on metals/dust

Table II: Dust Samples Collected in the Dust Filter in the Experiment VAMPYR-II [3].

Test	Dust (mg)				
	C	Fe	Ni	Cr	Total
VAMPYRII,3	88.9	8.7	9.4	3	110
VAMPYRII,4	18.1	6.8	1.8	0.9	27.6

3.2 Carbonaceous Dust (Binder)

To form a fuel compact or pebble, TRISO fuel particles and powdered high-purity graphite are mixed with about 10% of a binder material. The Processing temperature in such a case is limited to less than 2000 ℃ to protect against significant damage to the SiC coating of TRISO particles, which would allow uranium to diffuse into the graphite. However, high-temperature graphitization and purification requires a temperature of ≥ 2800 ℃. the binder in the fuel compact or pebbles is less-completely graphitized and less pure than the high-purity nuclear-grade graphite. Moreover, an incompletely-graphitized binder may be more active chemically [7]. Fig. 2 presents the atomic structures of both

graphite and amorphous carbon (binder). The graphite consists of three parallel graphene planes on which atoms are positioned in a hexagonal array, as obtained by the graphitization of carbon-based materials [8, 9]. The ''amorphous carbon'' has little graphitic order and consists of an aggregate of small crystallites, each of them consisting of a few graphite layer planes with some parallelism and many imperfections [10].

The properties of carbonaceous dust will be similar with black carbon comes from combustion. The reaction chain starts with the production of polycyclic aromatic hydrocarbons which serve as nuclei to form small spherical particles of a few nanometres with graphite layers [11]. These spheres coagulate to form a black carbon chain. Mixtures of carbon aerosol are of an external mixture type because the carbon particles are chemically pure and the mixtures consist of particles of different chemical compositions.
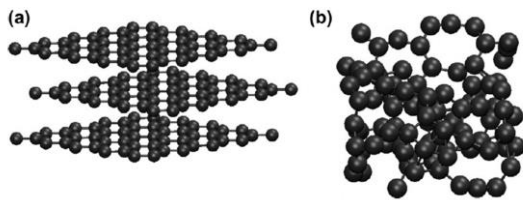
Fig. 2. Atomic structures of graphite and amorphous carbon [8].

3.3 Size

The size of the dust was measured at the end of the life of a pebble-bed AVR and found to be largely in the submicron range with a geometric-mean diameter of 0.6 μm [12]. IAEA-TECDOC-978 [3] provides a compilation of experimental and analytical data on the graphite dust from AVR and THTR. The report proposed the elementary dust particle sizes are small, with an average size of 0.8 μm from analysis of the historical AVR data. Analyses from the AVR and THTR plants showed that the dust occurred primarily in a range between 0.2 μm and 10 μm. Some random particles from wipes were found to be as large as 200 µm; however, the cumulative distribution of dust mass, as measured in AVR, was found to be 99% of less than 10 μm [13]. Experiments on the dust generated by the HTR-10 via pebble abrasion indicate a geometric-mean diameter of approximately 2.2 μm[14] with about 90% of the dust, in terms of the number of particles, being ≤ 6 μm in diameter.
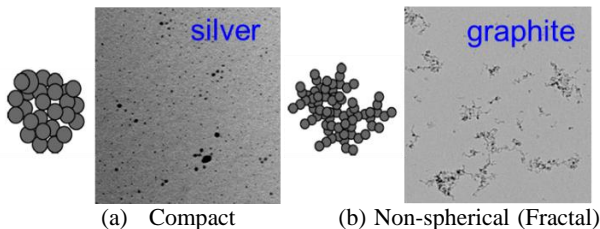
(a) Compact   (b) Non-spherical (Fractal)
Fig. 3. Typical type of aggregate and spark generated particles [6, 15].

3.4 Dust Morphology

There are two common types of aggregate particles described in the literature. The first type is a compact aggregate, whose external envelope is not far from spherical shape of silver particles (Fig. 3a). An example of the second type of aggregate particles for which the external envelope is highly non-spherical is the graphite particles (Fig. 3b). Such particles are often termed "fractal". These particles are of particular interest because they are highly irregular in nature, and have been studied extensively, both theoretically and experimentally [16]. These spheres coagulate to form various types of chains, but the typical type of aggregate can be defined as represented in Fig. 3.

The shapes of particles having a non-spherical structure can be characterized in terms of their fractal dimensions. Fractals are structures that have geometrically similar shapes at different levels of magnification, self-similarity. The fractal dimension links a property such as the perimeter or surface area of an object to the scale of the measurement. It is defined by the relationship between the numbers of primary particles in an aggregate and a characteristic radius, typically the radius of gyration [17]. The fractal dimension can vary between 1(a straight line) and 3 (a dense sphere). For compact agglomerates, the fractal dimension would be very close to 3. For aerosol particles, the value of the fractal dimension is distributed between 1.4 and 2.5 [18].

4. FP-Dust Interaction

The FP and dust interaction can be divided into two steps. The primary interaction step is between a pure FP and a normal dust as shown in Fig. 1. The secondary interaction step will be between a FP bored dust and a normal dust or between the both FP bored dusts. The primary interaction occurs earlier and more rapidly than the secondary interaction. The primary interaction will occur near the nuclear fuel. The FP elements or chemical compounds leaking from TRISO and from fissions of Uranium impurities in graphite matrix material are absorbed into the graphite of the fuel compact or pebbles. These absorbed FPs are slowly released due to vapour pressure or rapidly released when the core heats up. These phenomena can then be considered as released FP attached (coagulation) to suspended dust in the primary coolant. Of course, the FP can diffuse into the pebbles or fuel compact surfaces, absorb into crushed surface of the graphite (by friction, abrasion, collision, vibration, etc.) and drop onto the wall or become suspended on the primary coolant. However, this can be simplified if the FP absorbed into graphite comes off with the dust.

It is well known that the behaviour of FP adsorbed into dust greatly depends on the physico-chemical properties of the FP [19, 20]. The major property effect on the interaction is the vapour pressure of FP. For instance, because the boiling point of Cesium is 705 ℃, it is predictable that it will scarcely stay in the dust while passing through the primary system. On the other hand, Silver will be able to stay in the dust owing to its high melting point. In the case of Strontium which has a melting point of 769 ℃, it can be liquefied and slightly separated from the dust when passing through the core. Some chemical reactions can occur if Strontium collides with impurities in the coolant, such as oxygen or hydrogen as well as FP-dust suspended through the coolant in a chemical compound form. Previously produced FP which is leaked from the pebbles or fuel compact will be adhere to any component of the RCS or become suspended and circulate in the RCS according to the mass conservation law, either until all FPs are decayed or until this material is captured by a filter in a helium purification system (HPS). Although HPS filters dust larger than 5µm in general, it is highly likely that the dust will adhere to a reactor component of the RCS before filtering because it takes approximately one day for all of the coolant to pass through the HPS. When considering that the helium speed of the primary system is generally 30 m/s under normal operation,

one cycle of circulation of coolant through the RCS takes approximately 2 or 3 seconds. It is obvious that Iodine, with a boiling point of 100 ℃, turns into a gas and becomes detached from suspended dust not only when it passes through the reactor core, but also when it passes through low-temperature piping at 350 ℃.

4.1. Dust Behaviour

4.1.1. Lognormal Size Distribution

Many particles are unstable. They can change by growing or can even disappear upon contact with a surface, coalescing or as an ion losing its charge after contact with a surface or an oppositely charged particle (radioactive aerosols). This chapter provides the background and introductory information about aerosol behaviour. It is common to report aerosol size data in terms of the parameters of the lognormal size distribution regardless of whether the aerosol satisfies the criteria of a lognormal distribution being a good approximation of the actual size distribution. Many experimental results indicate that particle size distributions during coagulation fit approximately a lognormal function. It is concordant to the size distribution of AVR dusts as shown in Fig. 4 [21].
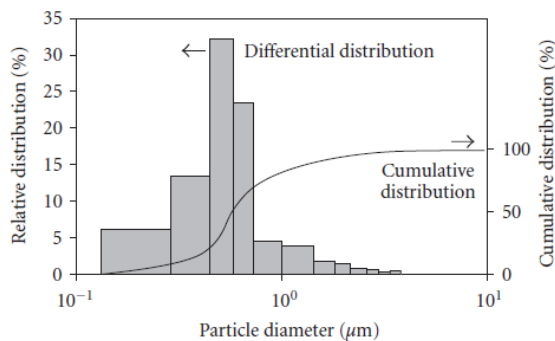
Fig. 4. Number weighted size distribution of AVR dust.

4.1.2. Particle Motion

Generally, aerosol particles are divided into three regimes according to their sizes of particles ranging from $10^{-3}\mu m$ to 100 μm in equivalent radius. These regimes of aerosol behaviour are usually categorized in terms of the Knudsen number (K_n) which is the ratio of the mean free path (λ) of gas molecules to the particle diameter:

$$K_n = \frac{2\lambda}{d_p} \qquad (1)$$

If $K_n < 0.1$, continuum behaviour is approached and,
If $K_n > 10$, free molecular flow is approached.

This number relates the particle diameter (d_p) to the mean distance travelled by an air molecule between collisions, or mean free path. At high Knudsen numbers, the aerosol particles are in the free molecular flow regime and experience forces that depend on the Maxwell–Boltzmann molecular speed distribution, while at low Knudsen numbers the particle is many mean free paths in size, and the gas acts as a continuous fluid regime. When the Knudsen number is neither high nor low, the particles are considered in the transition regime. In this regime, the particle transport exhibit characteristics of both free molecular and continuous fluid regimes.

4.1.3. Coagulation Dynamics

Coagulation greatly affects the size and consequently the mobility of aerosol particles, such that aerosol particles quickly develop a size distribution. Particles coagulate because they cross stream-lines of the flow to come into contact. There are a variety of mechanisms that can cause particles to cross stream-lines. Each of these mechanisms is characterized by a distinct collision kernel. The more common collision kernels recognized in models of aerosol growth during reactor accidents are as follows:

Gravitational: Larger particles sweep out smaller particles as they fall under the force of gravity.
Brownian diffusion: Fluctuations in molecular bombardment drive particles across streamlines of the flow to come into contact with other particles
Turbulent diffusion: Turbulent eddies carry particles across streamlines to come into contact with other particles.
Turbulent inertia: Particles expelled from turbulent eddies impact other particles.
Charge: Charged particles enhance the coagulation or repulse neighboring particles.

The simplest comparison results (without a charge) between the various collision kernels are shown in Fig. 5 [18], in which one particle is taken to have a fixed diameter of 1.0 μm while the other diameters vary under a particular set of circumstance. It is clear that Brownian diffusion results in the highest collision rates for particles less than 1.0 μm in diameter, whereas for larger particles, kinematic (turbulent) diffusion and differential settling (gravitational) become much more important. As the size of the second particle becomes greater than a few micrometres, the collision rate due to sedimentation increases sharply and becomes comparable to the shear-induced rate (turbulent inertia). Of course, results such as those presented in Fig. 5 depend on certain assumed conditions. The various collision rate constants are affected in different ways by colloidal and hydrodynamic interactions.
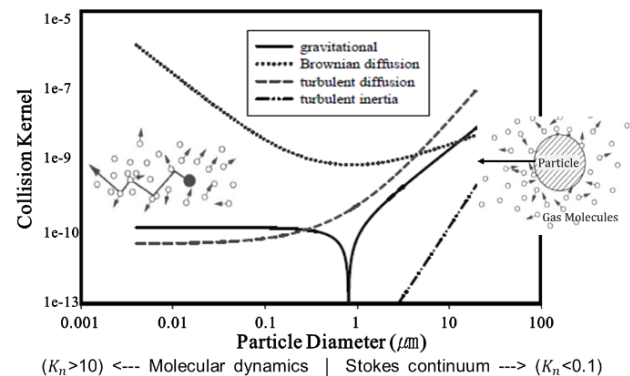
Fig. 5. Comparison of collision kernels for various mechanisms of coagulation [18].

4.1.4. Self-preserving Size Distribution

The coagulation of monodisperse aerosols will gradually lead to a polydisperse aerosol, as some particles become larger and undergo enhanced coagulation. Theoretical analyses [22] of the competing mechanisms of narrowing and broadening suggest that a stable size distribution will form after a long time, regardless of the initial size distribution. The resulting size

distribution is known as the self-preserving size distribution and is approximately lognormal with a Geometric Standard Deviation in an approximate range of 1.32 to 1.36. As a practical matter, long times are required for aerosols to reach self-preserving size distributions as shown in Fig. 6 based on an analysis by Park et al. [23] and Maynard & Zimmer [24], unless the aerosol has a small initial particle size, a very high initial number concentration, and a relatively narrow initial size distribution.
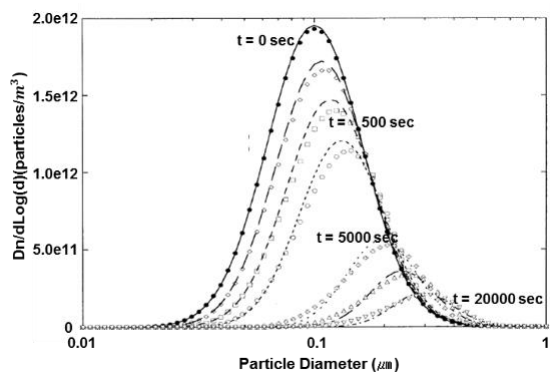
Fig. 6. Effect of coagulation on the particle size distributions [23, 24].

4.2. FP Sticking Rate to Dust

Skyrme [25] carried out theoretical work on the attachment of gaseous FPs to aerosol particles. He estimated the FP sticking rates under various conditions, finding that the concentration of FPs in the gas phase diminish within a container as a result of deposition on monodispersed and polydispersed populations of aerosol particles. The trends of time constant, derived by his theoretical analysis, are represented in Fig. 7 for the reduction in the FP concentration due to absorption by monodispersed particles with the radius, concentration and sticking probability. These results indicate that FPs can be expected to attach to dust particles, that this is more likely to occur with smaller particle sizes, and that it occurs rapidly: in most circumstances, the time constant for attachment to dust particles is shorter than that for attachment to surfaces as shown in Table III. Dust size proved an important factor with regard to FPs sticking to suspended dust. The size dependence indicates that small particles may carry a disproportionately large quantity of FPs. An example is given for a typical polydispersed lognormal distribution of particles, in which only 6% of the total mass is in particles below $0.5\mu m$ in diameter, but these particles carry 64% of the FPs. He concluded also that for a significant concentration of submicron particles in a large container, the deposition of gaseous FPs onto particles is far more rapid than that onto the container walls. Moreover, if considering self-charged FP-dust, the size growth of the dust is suppressed due to the generation of strong repulsive electrostatic forces, as explained in section 4.3. The size of charged dust will be smaller than the size of dust according to Skyrme's theoretical analysis. Accordingly, the charged FPs will be more efficient for FP attachment to an aerosol or dust.

4.3. Aerosol Models in Current Plateout Codes

Dust concentration is one of important variables in both FP plateout models at the normal operating condition and FPs release scenarios during depressurization accidents. Most of plateout design codes developed before 2000th which ignored the presence of dusts do not consider aerosol models such as PADLOC [26], PLAIN [27] and SPATRA [28]. Later, an analysis has been performed for the 500 MW NGNP PBR demonstration power plant using SPECTRA [29], which has the aerosol models of sectional approach. The SPECTRA code can derive the dust concentration based on mechanistic aerosol model. If the dust size distribution is assumed as a constant, the dust concentration can be obtained simply. This approach is referred to as the bulk aerosol model and most of plateout codes adopted this bulk aerosol model such as PATRAS [1], RADAX [30] and DAMD [31].

Table III: Theoretical Assessment of the Sticking Rates of FPs to Dust and Walls.

Dust Behaviour		Time
Gases FP absorb on dust	Single dust	$< \sim \mu$ sec
	Monodispersed dust	< 10 sec
	Polydispersed dust	$> \sim \mu$ sec
Agglomeration	Brownian effect only	$\gg 10$ sec
Gases FP to wall	Uniform distribution	< 100 sec
Plateout on wall	Gravity	$0 \sim$ infinite
	Turbulent	~ 10 sec
	Brownian diffusion	> 1000 sec
	Thermophoresis	~ 1000 sec
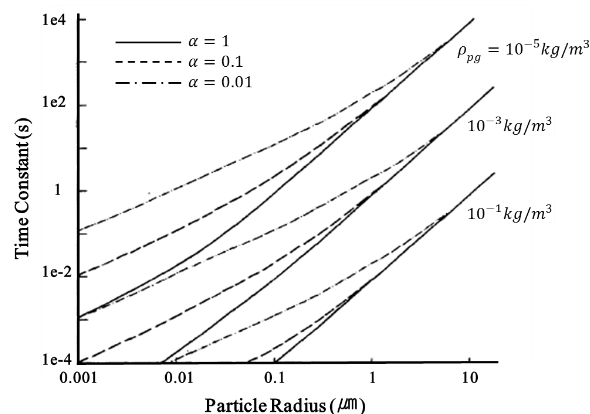
Fig. 7. Time constant for the reduction in the FP concentration due to absorption by monodispersed dust (ρ_{pg}: concentration, α: sticking probability).

5. Summary

FPs generated from fission are nano-sized particles. Suspended dust, previously formed in the RCS by various reactions, is the carrier that moves the FP out of the core. In general, the dust is much larger than the FP and will be distributed at a polydispersed distribution. There are two factors that make the interaction complicated. One is diverse forms of both FP and dust. The diversity of the FP, is determined by its unique physico-chemical properties while diversity of dust is due to its various sizes as well as the substances it contains. The other factor, which is the concentration of the dust, depends on the part of the primary system of the reactor in which the dust is located.

The FP and dust interaction can be divided into two steps. The primary interaction step is between a pure FP and a normal dust. The secondary interaction step will be between a FP bored dust and a normal dust or between the both FP bored dusts. The

primary interaction occurs earlier and more rapidly than the secondary interaction. The primary interaction will occur near the nuclear fuel. The FP elements or chemical compounds leaking from TRISO and from fissions of Uranium impurities in graphite matrix material are absorbed into the graphite of the fuel compact or pebbles. These absorbed FPs are slowly released due to vapour pressure or rapidly released when the core heats up. Secondary interactions can be predicted using a well-established system from the aerosol or colloid field. The typical mechanisms of particle coagulation vary with the particle size. Dust coagulation occurs due to particle collisions arising from their differing velocities. Particle motion is induced by Brownian diffusion, sedimentation and turbulence with other influences such as electrical forces. The basic framework of physico-chemical modelling is well established because the research on interactions with dust is academically well developed in the field of aerosols. However, existing correlations or coefficients of previous models cannot be applied directly to the very dry circumstances at high temperature and high pressure conditions of HTGR. This can be resolved by additional experiments with analytical modelling of the required condition.

Gaseous dust can become charged through aerosol-generation processes, FP decay, and an ionizing environment. FP-dust will be effectively self-charged over the life of the radioactive FPs they contain. The charge on the dust modifies the FP-dust coagulation rate by generating electrostatic interactions. Thus, particle charging and coagulation can mutually affect each other and simultaneously affect both the charge and size distributions in the RCS. The aggregation rates of slightly radioactive gold particles can be up to five times lower than those of non-radioactive gold particles due to the repulsive electrostatic forces caused by the self-charging effect. The size growth of the particles by coagulation was suppressed due to the generation of strong repulsive electrostatic forces. Practically in nuclear aerosol analyses under an accident condition of a LWR, The charging effect is not important because the charge effects are minimized due to the high humidity, therefore these analyses are not designed to consider charged aerosols. For this reason, additional work is needed with regard to nuclear aerosol analyses of dry HTGR systems to gain insight into the current progress on charged FP aerosols.

Conceptually, it is evident that if the concentrations of circulating and deposited dust in the circuit are very low then dust effects should be unimportant. In the other extreme, if the concentrations of dust are very high, then dust effects should play a dominant role in determining the transport, deposition and re-entrainment behaviour of FPs. The circulation of large quantities of graphite dust in the primary coolant loop of PBRs has the potential to adversely affect the operation of the reactor components. This would be a significant disadvantage for the PBR. The PMR concept also has a clear advantage in that it involves fewer uncertainties with respect to dust in the primary coolant circuit. Dust concentration is one of the important variables in both FP plateout model at the normal operating condition and FPs release scenarios during depressurization accidents. A successful analysis of this type has been performed for the 500 MW NGNP plant (Westinghouse pebble bed design) using SPECTRA, which has the aerosol models of sectional approach.

6. Recommendations of Useful FP-dust Interaction Codes

Since its introduction by Gelbard and co-workers in 1980 [32], the sectional model remains one of the best performing methods in computational simulation of simultaneous coagulation and deposition without condensation. The most widely used coagulation model for confined atmospheres is the MAEROS code [33], which have been implemented in the nuclear accident analysis codes, MELCOR [34] and SPECTRA. The sectional method is used in the MAEROS code and it has been incorporated in many thermal hydraulic applications to assess the accidental nuclear source term, and in other applications where changes in particle size distribution are of interest. Recently, Geng et al. [35] proposed a versatile computer model, SEROSA, which permits an arbitrary number of sections with arbitrary size boundaries to simulate the temporal evolution of coagulation and deposition under multiple flow-regimes and coagulation types. They are benchmarked against an analytical model as well as three coagulation models, MAEROS, COAGUL [36], and NGDE [37], using coincident section boundaries and coagulation mechanisms.

REFERENCES

[1] N. Iniotakis, and C. B. vonder Decken, The Influence of Dust on the Behaviour of Fission Products in High Temperature Reactors, ENS/ANS Topical Meeting on Nuclear Power Reactor Safety, Brussels 16-19, 1978.
[2] INL/EXT-10-17997, Mechanistic Source Terms White Paper, U.S. DOE, Idaho Falls, 2010.
[3] IAEA TECDOC-978, Fuel Performance and Fission Product Behaviour in Gas Cooled Reactors, INIS Clearinghouse, Vienna, Austria, 1997.
[4] T. Burchell, R. Bratton, W. Windes, NGNP Graphite Selection and Acquisition Strategy, ORNL, 2007.
[5] R. S. Troy et al., Generation of Graphite Particles by Sliding Abrasion and Their Characterization, Nuclear Technology Vol. 189, 2015.
[6] M. P. Simones et al., Measurements of Aerosol Charge and Size Distribution for Graphite, Gold, Palladium, and Silver Nanoparticles, Nuclear Technology Vol. 176, 2011.
[7] K. Y. Wen, T. J. Marrow, B. J. Marsden, The microstructure of nuclear graphite binders. Carbon 46 (1), 62–71, 2008.
[8] Londono-Hurtado et al., A Review of FP Sorption in Carbon Structures, J of Nuclear Materials, 2012.
[9] T. D. Burchell, Carbon Materials for Advanced Technologies, Pergamon, 1999.
[10] H. O. Pierson, Handbook of Carbon, Graphite, Diamond, and Fullerenes Properties, Processing, and Applications, Noyes Publications, Park Ridge, NJ, 1993.
[11] T. C. Bond et al., Bounding the Role of Black Carbon in the Climate System: a Scientific Assessment, J Geophys Res 118:5380–5552, 2013.
[12] H. Gottaut and K. Kruger, Results of Experiments at the AVR reactor. Nuclear Engineering and Design, 121, 143-153, 1990.
[13] VDI, "AVR - Experimental High-Temperature Reactor, 21 Years of Successful Operation for a Future Energy Technology," the Society for Energy Technologies, pp. 9–23, 1990.
[14] X. W. Luo, S. Y. Yu, X. Sheng, Temperature Effect on IG-11 Graphite Wear Performance, Nuclear Engineering and Design, 235 (21), 2261–2274, 2005.

[15] P. F. DeCarlo et al., Particle Morphology and Density Characterization by Combined Mobility and Aerodynamic Diameter Measurements. Part 1: Theory, Aerosol Science and Technology, 38:1185–1205, 2004.

[16] K. Park, D. Kittelson, P. McMurry, Structural Properties of Diesel Exhaust Particles Measured by Transmission Electron Microscopy (TEM): Relationships to Particle Mass and Mobility, Aerosol Sci. Technol., 38(9):881–889, 2004.

[17] S. K. Friedlander and D. Y. H. Pui, Emerging Issues in Nanoparticle Aerosol Science Technology, J. Nanoparticle Res. 6(2):313–320, 2004.

[18] NEA, State-of-the-Art Report on Nuclear Aerosols. NEA/CSNI/R(2009)5, 2009.

[19] R. Moormann and K. Hilpert, Chemical Behaviour of Fission Products in Core Heatup Accidents in High-Temperature Gas-Cooled Reactors Nuclear Reactor Safety, Nuclear Technology Vol. 94, 1991.

[20] M. P. Kissane, A Review of Radionuclide Behaviour in the Primary System of a Very-high-temperature Reactor. Nuclear Engineering and Design, Vol. 239, pp. 3076-3091, 2009.

[21] Zimmermann, E. and Ivens, G (1997), Abschlussbericht über den Leistungsbetrieb des AVR-Versuchskraftwerks Jül-3448 Forschungszentrum Jülich, pp. 297, ISSN 0944-2952.

[22] S. K. Friedlander, Smoke, Dust and Haze, John Wiley & Sons, New York, 1977.

[23] S. H. Park et al., The Log-Normal Size Distribution Theory of Brownian Aerosol Coagulation for the Entire Particle Size Range: Part I, Analytical Solution Using the Harmonic Mean Coagulation Kernel, J. Aerosol Sci. 30(1):3–16, 1999.

[24] A. D. Maynard and A. T. Zimmer, Development and Validation of a Simple Numerical Model for Estimating Workplace Aerosol Size Distribution Evolution through Coagulation, Settling, and Diffusion, Aerosol Science and Technology, 37:804–817, 2003.

[25] G. Skyrme, Attachment of Gaseous Fission Products to Aerosols, Fission Product Release and Transport in Gas-Cooled Reactors, (Proc. IAEA Specialists Meeting, Berkeley, 1985), IAEA IWGGCR/13, Vienna 262-274, 1985.

[26] W.W. Hudritsch and P. D. Smith, PADLOC, A One-dimensional Computer Program for Calculating Coolant and Plateout Fission Product Concentrations, GA-A14401, 1977.

[27] O. Baba, N. Tsuyusaki, K. Sawa, Fission Products Plate-out Analysis Code in the HTGR, JAERI-M-88-266, 1988.

[28] R. Moormann, Source Term Estimation for Small-Sized HTR's, Research Center Julich, Report July-2669, 1992.

[29] M. M. Stempniewicz, SPECTRA—Sophisticated Plant Evaluation Code for Thermal-hydraulic Response Assessment, Version 3.60, NRG, 2010.

[30] L. Stassen, Validation of the Plate-out Model in the RADAX Code Used for Plate-out and Dust Activity Calculations at PBMR. Advances in Nuclear Analysis and Simulation, PHYSOR, 2006.

[31] C. C. Stoker, PBMR Radionuclide Source Term Analysis Validation Based on AVR Operating Experience, Nuclear Engineering and Design 240, 2010.

[32] F. Gelbard and J. H. Seinfeld, Simulation of Multicomponent Aerosol Dynamics, J. Colloid Interface Sci. 78(2):485-501, 1980.

[33] F. Gelbard, MAEROS User Manual, NUREG/CR-1391, Sandia National Laboratories, 1982.

[34] NUREG/CR-6119, MELCOR Computer Code Manuals: Vol. 2. Reference Manuals (Version 1.8.5), U.S. NRC, 2000.

[35] J. Geng, H. Park, E. Sajo, Simulation of Aerosol Coagulation and Deposition under Multiple Flow Regimes with Arbitrary Computational Precision, Aerosol Science and Technology, 47:530–542, 2013.

[36] S. H. Suck and J. R. Brock, Evolution of Atmospheric Aerosol Particle Size Distributions via Brownian Coagulation: Numerical Simulation, J. Aerosol Sci., 10:581–590, 1979.

[37] A. Prakash, A. B. Bapat, M. R. Zachariah, A Simple Numerical Algorithm and Software for Solution of Nucleation, Surface Growth, and Coagulation Problems, Aerosol Sci. Technol., 37:892–898, 2003.